Accepted Manuscript

Distribution of dissolved and leachable particulate Pb in the water column along the GEOTRACES section GA10 in the South Atlantic

Christian Schlosser, Johannes Karstensen, E. Malcolm S. Woodward

PII: S0967-0637(19)30090-1

DOI: https://doi.org/10.1016/j.dsr.2019.05.001

Reference: DSRI 3041

To appear in: *Deep-Sea Research Part I*

Received Date: 20 March 2019

Revised Date: 30 April 2019

Accepted Date: 2 May 2019

Please cite this article as: Schlosser, C., Karstensen, J., Woodward, E.M.S., Distribution of dissolved and leachable particulate Pb in the water column along the GEOTRACES section GA10 in the South Atlantic, *Deep-Sea Research Part I* (2019), doi: https://doi.org/10.1016/j.dsr.2019.05.001.

Distribution of dissolved and leachable particulate Pb in the water column along the GEOTRACES section GA10 in the South Atlantic

Christian Schlosser[1,*], Johannes Karstensen[1], and E. Malcolm S. Woodward[2]

[1]GEOMAR Helmholtz-Centre for Ocean Research Kiel, Wischhofstr. 1-3, 24148 Kiel, Germany

[2] Plymouth Marine Laboratory, Prospect Place, PL1 3DH, Plymouth, United Kingdom

*corresponding author: Schlosser.chr@gmx.de

For submission to Deep-Sea Research Part I: Oceanographic Research Papers

Abstract

We measured concentrations of dissolved and leachable particulate lead in the water column along a 40°S zonal transect in the South Atlantic Ocean, as part of the international GEOTRACES section GA10. Dissolved Pb (DPb) concentrations were highest in surface waters (8 – 29 pmol L^{-1}) and lowest near the sea floor (< 5 pmol L^{-1}). Estimates for mineral sourced DPb for the South Atlantic surface ocean yielded a concentration of 5 ± 1 pmol L^{-1}, suggesting that about 59% of the 12 ± 2 pmol L^{-1} (n = 85) DPb present in today's South Atlantic surface ocean has come from anthropogenic sources. Available values for wet deposition of 14 ± 12 nmol Pb m^{-2} d^{-1} (Chance *et al.*, 2015) allow the calculation of an average residence time of 35 ± 31 days for DPb in the South Atlantic surface ocean. Elevated concentrations of LpPb, reaching 28 pmol L^{-1}, were restricted to turbid bottom waters on the South American shelf and in the Argentine Basin, suggesting that strong turbulent mixing and resuspension of sediments was the main source of this Pb fraction. A negative linear regression between LpPb and DPb in these turbid waters indicated that the main removal mechanism for DPb in bottom waters on the shallow South American shelf and in nepheloid layers in the abyssal planes of the Argentine basin was the scavenging of DPb onto the surfaces of resuspended sediment particles.

Elevated DPb concentrations in surface waters near the South African (23 ± 3 pmol L^{-1} (n = 22)), and South American (18 ± 3 pmol L^{-1} (n = 14)), continental margins coincided with the position and extension of the Agulhas (AC) and Brazil Current (BC). Elevated DPb concentrations of 12 ± 1 pmol L^{-1} (n = 30) at depth in the Argentine Basin (the western basin of the 40°S transect) coincided with the spreading of North Atlantic Deep Water (NADW) in the depth range of 1,750 to 3,000 m. Lowest DPb concentrations of 5 ± 1 (n = 26) and 6 ± 1 pmol L^{-1}

(n = 22) corresponded with Weddell Sea Deep Water and Antarctic Bottom Water, located below NADW in the Argentine and Cape Basins (the eastern basin of the 40°S transect).

Keywords: Lead (Pb); Trace Metals; GEOTRACES; South Atlantic; Biogeochemical Cycles

1. Introduction

Lead (Pb) is a heavy metal and anthropogenic emissions to the atmosphere result in elevated concentrations in the environment (Krause *et al.*, 1993; Boyle *et al.*, 2014; Echegoyen *et al.*, 2014). Anthropogenic Pb emissions peaked in the 1970s due to the combustion of tetraethyllead (TEL) in leaded gasoline and by high temperature combustion in coal burning power plants and ore smelters (Damle *et al.*, 1981; Cziczo *et al.*, 2009; Engineering, 2011; European Environment Agency, 2018). These artificial airborne particles are generally very small (50 nm to 1 μm (Murphy *et al.*, 2007)) and therefore tend to be transported in the atmosphere over greater distances than mineral dust particles, which are generally larger than 1 μm (Mahowald *et al.*, 2018). This enables the transport of anthropogenic Pb to remote open ocean regions (McConnell *et al.*, 2014) and increases the concentration of dissolved Pb (DPb) in the marine environment (Kelly *et al.*, 2009).

Information from banded coral archives suggest that pre-industrial dissolved Pb (DPb_{pre}) concentrations in the North Atlantic surface ocean near Bermuda were roughly 15 pmol L^{-1} (Shen and Boyle, 1987; Lima *et al.*, 2005; Kelly *et al.*, 2009). Surface waters collected at the Bermuda Atlantic Time-series Study (BATS) site during the 1970s (peak in anthropogenic Pb emissions) contained circa 200 pmol DPb L^{-1} (Boyle *et al.*, 2014). Together this suggests that just 7% of the DPb at BATS in the 1970s came from mineral dust (Pb_{min}), while 93% came from anthropogenic sources (Pb_{anth}), most likely located in North America and Europe (Boyle *et al.*, 2014). The effectiveness of beginning to ban TEL in the 1970th (a process still ongoing in Yemen and Algeria (Akumu 2019)) and of restricting emissions related to other anthropogenic sources (European Environment Agency, 2018) is clear from the drop in DPb concentrations in North

Atlantic surface waters down to present day values of around 20 pmol DPb per liter of seawater (Noble *et al.*, 2015; Zurbrick *et al.*, 2018).

As with other such accidental introduced tracers, like chlorofluorocarbons (Fine 2011), anthropogenic Pb is making its way into the ocean interior. Even though DPb is quickly removed from surface seawater by scavenging onto particle and colloidal surfaces (Helmers and van der Loeff, 1993; Luengen *et al.*, 2007; Chuang *et al.*, 2014; Yang *et al.*, 2015), DPb levels of roughly 50 pmol L^{-1} can be found at 20°N between 800 and 2,000 m depth in the North Atlantic, related to spreading of North Atlantic Deep Water (NADW) formed roughly 50 years ago (GEOTRACES, IDP 2017, GA02 & GA03 (Noble *et al.*, 2015; Schlitzer *et al.*, 2018)). Elevated DPb concentrations of similar magnitude have been reported for Subantarctic Mode Water in the Indian Ocean (Lee *et al.*, 2015), waters of the Agulhas Current in the South Atlantic (Paul *et al.*, 2015), for Pacific Deep Water in the Chinese Sea (Chen *et al.*, 2016; Chien *et al.*, 2017), for Mediterranean Overflow Water (MOW) in the West Atlantic (Noble *et al.*, 2015; Rusiecka *et al.*, 2018; Zurbrick *et al.*, 2018) and deep Antarctic waters in the Indian sector (Boyle *et al.*, 2014), all suggesting that DPb can be used as a useful water mass tracer. Meanwhile, reduced DPb concentrations in younger MOW and NADW (Zurbrick *et al.*, 2018), reflects the decline in anthropogenic Pb emissions with stricter environmental regulations (European Environment Agency, 2018).

Although we have gained a lot of knowledge about the past and present distribution of Pb in the North Atlantic and North Pacific Oceans, less is known about DPb in the oceans of the Southern Hemisphere, especially at mid- to high latitudes. In this study, we present the concentrations of DPb and leachable particulate Pb (LpPb) along the GEOTRACES section GA10 in the South Atlantic, following the 40°S parallel. In addition, we present estimates for

95 Pb_{min} and Pb_{anth} of the South Atlantic surface ocean, estimate the residence time for DPb in
96 surface waters, and discuss the interaction between DPb and LpPb. Lastly, we identify water
97 masses with characteristic DPb concentrations.
98
99 **2. Methods**
100 *2.1 Water sampling*
101 Seawater samples for Pb analysis were collected during two UK GEOTRACES cruises
102 sampling the GA10 section in the South Atlantic Ocean, from Cape Town, South-Africa to
103 Montevideo, Uruguay. The first cruise took place in October/November 2010 on RRS *Discovery*
104 (D357, Figure 1: grey circles, covering St. 1 to St. 6, additional station 4.5 and 2.5 contain only
105 temperature, salinity, and nutrient data). The cruise was restricted to the eastern part of the Cape
106 Basin due to a medical evacuation. The second cruise took place the following year, from
107 December 2011 to January 2012 on RRS *James Cook* (JC068 Figure 1: black circles, covering
108 repeat station 1 to 3 and station 7 to station 24) and completed the zonal transect. Due to
109 challenges with the conductivity-temperature-depth (CTD) water sampling device, station
110 numbers 10 and 23 were excluded.
111 During JC068, 113 surface samples were collected using a tow-fish deployed from the
112 starboard side of the ship at 3 – 4 m water depth. The seawater was pumped through a completely
113 enclosed acid-cleaned polyvinylchloride (PVC) tubing system into a class 100 clean laboratory
114 container using a Teflon bellows pump (Almatec E-Series). Dissolved samples were filtered
115 inline through a staggered cartridge filter (0.8/0.2 µm, AcroPak1000™) and collected in acid-
116 cleaned low density polyethylene (LDPE, Nalgene) sample bottles for later analysis.

Vertical profiles with a maximum of 24 DPb and 12 total dissolvable (TDPb, unfiltered) samples were collected at each of the 19 full depth stations using 24 trace metal clean 10 L Niskin bottles (Ocean Test Equipment, USA) mounted on a titanium frame rosette. The associated CTD was attached to a non-conductive Kevlar cable, and the Niskin bottles were triggered at programmed depths using an automated-firing-module (AFM, Seabird). After recovery, the bottles were carried into the sampling laboratory container, clamped, and connected to a pressure hose providing filtered compressed air (0.2 – 0.3 bar) from a 50 L gas bottle. Dissolved samples were filtered through a staggered cartridge filter (0.8/0.2 µm, AcroPak500™) into acid washed LDPE sample bottles. Unfiltered samples were directly dispensed in acid washed LDPE sample bottles. Dissolved and total dissolvable samples were acidified with concentrated ultra-purity hydrochloric acid (HCl, Romil, UpA) to pH 1.9 (~0.016 mol H^+ L^{-1}), were stored in the dark, and shipped for later analysis at the National Oceanography Centre, Southampton, UK. Leachable particulate Pb (LpPb) was determined as the difference between DPb and TDPb (i.e., LpPb = TDPb – DPb).

During D357, between 12 and 24 DPb subsurface samples were collected at each of the 6 full depth stations as described for JC068. The sampling depth ranged from 10 to 400 m on the shallow South African shelf and from 20 to 5.100 m in the Cape Basin. Total dissolvable Pb samples (unfiltered) were not collected during D357.

2.2 Analysis

Concentrations of Pb in seawater samples were analyzed by off-line preconcentration and isotope dilution inductively coupled plasma – mass spectrometry (ID-ICP-MS) following a modified method outlined by Rapp et al. (2017). In short, approximately one year after collection, 12 mL of seawater that had been acidified upon collection was transferred into 30 mL

acid-washed fluorinated ethylene propylene (FEP) bottles and spiked with a solution containing mainly ^{207}Pb. Samples were irradiated for 3.5 hours with strong ultraviolet light to destroy metal chelating compounds. The sample solution was buffered to pH 6.4 using a 2 M ammonium acetate solution made by mixing ammonia and glacial acetic acid (both 'Fisher Optima' grade). The resulting solution was immediately preconcentrated using a half-automated system (Preplab, PS Analytical) equipped with a 2 cm mini column (GlobalFIA) filled with a metal chelating resin (WACO) (Kagaya *et al.*, 2009). Any salts remaining on the resin were rinsed away using deionized water (18.2 MΩ cm, MilliQ, Millipore). In the following step, retained metals on the resin were eluted in acid cleaned 4 mL polypropylene vials using 1 mL of a 1 M sub-boiled HNO_3 solution. The collected vials were placed into the auto-sampler (Elemental Scientific) of the ICP-MS (Element XR, Thermo Finnigan).

Certified seawater standards (SAFe S, SAFe D2 and GEOTRACES S, GEOTRACES D) were preconcentrated and analyzed with each batch of samples, in order to validate our measured sample concentrations. Values obtained agreed with reported values for the GEOTRACES and the SAFe reference material (Table 1). The analytical error corresponds to 1 standard deviation (1 s.d.) of the uncertainty of the ICP analysis and mass bias correction. The precision for replicate analyses was between 1 – 3%. The method blank (sum of Pb contribution from the buffer and manifold device) and the limit of detection (LOD, three times the standard deviation of the blank) for Pb are listed in Table 1.

Unfiltered seawater for macronutrient analysis was dispensed into HCl cleaned, aged, high density polyethylene (HDPE) bottles using clean sample handling techniques according to the GO-SHIP nutrient protocols (Hydes *et al.*, 2010). All collected samples were analyzed immediately on board using either a colorimetric segment flow nutrient AutoAnalyzer (Bran

Luebbe) for micromolar concentrations (Woodward and Rees, 2001) or a segmented flow colorimetric analyzer with a 2 meter liquid waveguide flow-cell (Zhang and Chi, 2002) for nano-molar phosphate concentrations.

An extended Optimum Multiparameter (eOMP) analysis was conducted to identify water masses fractions and bulk remineralization/respiration for the water masses below 500 m depth (supp. Figure S1) (García-Ibáñez *et al.*, 2018). We used the Matlab™ package Version 2 available on the internet (omp.geomar.de). Water mass parametrization and parameter weighting are described in detail in the suppl. Text S1.

3. Results

3.1 Hydrographic settings

Two coastal surface water masses were identified during the cruise transect: the warm (15 – 25°C) and salty (35 – 37 PSU) Brazil Current (BC) near the South American margin and the warm (15 – 23°C) and less salty (34 – 35 PSU) Agulhas Current (AC) near the South African margin (Figures 1A & 1B). The Brazil and Agulhas Current were both easily discernible down to 400 – 500 m depth and were depleted in dissolved inorganic phosphorous (DIP < 0.2 μmol L^{-1}) (Figure 1C), and dissolved inorganic nitrogen (not shown in the figure).

After arising from the westward flowing South Equatorial Current further north at 10°S (Stramma *et al.*, 1990), the southward flowing Brazil Current deflects towards the east at the Brazil-Malvinas Confluence at around 40°S (McCartney, 1977; Stramma *et al.*, 1990), forming the South Atlantic Current (SAC), the southern branch of the South Atlantic Gyre (SAG).

The Agulhas Current, which has arisen from the East Madagascar Current and the Mozambique Current in the Indian Ocean sub-gyre (Stramma and Lutjeharms, 1997), splits near

the South African margin. Part of it becomes the Benguela Current (not shown) in the eastern South Atlantic and part retroflects at 15°E to merge with the eastward flowing Antarctic Circumpolar Current (ACC) (Figure 1A).

Two additional surface features are visible in the transect near the South American coast. A pronounced surface salinity minimum (< 28 PSU) exists on the South American shelf, corresponding to the input of freshwater from the La Plata River (supp. Figure S2), and shoaling of the nutricline and isotherms by two anticyclonic eddies is also visible by their sea surface height anomaly along the section between 40°W and 50°W (Figure 1C, S3).

Two upper layer water masses within the top 400 – 500 m of the water column were visible outside of the continental margins: the warm (>16°C) and salty (~35.5 PSU) Subtropical Surface Water (STSW) in the Argentine Basin, and the colder (<16°C) and fresher (~34.5 PSU) Subantarctic Surface Water (SASW) in the Cape Basin (Figure 1A & 1B). These water masses join at the Subtropical Front (STF) at roughly 40°S, where northeastward flowing SASW from the Antarctic Circumpolar Current (ACC) mix with westward flowing STSW (Stramma and Peterson, 1990) (Figure 1A). The STF represents an important transition zone, where the availability of DIN and DIP shifts from depleted in the north to replete in the south. The latitudinal position of the STF changes seasonally and at the time of the cruise it was south of 40°S in the Argentine Basin and north of 40°S in the Cape Basin (Figure 1A).

Two subsurface water masses were identified in the depth range between 500 and 1,750 m depth: Antarctic Intermediate Water (AAIW) overlying Upper Circumpolar Deep Water (UCDW). At 40°S, the AAIW was located between 500 and 1,250 m water depth, identifiable from its prominent salinity minimum of ~34.2 PSU (Figure 1B and supp. Figure S1). Upper Circumpolar Deep Water occurs below AAIW, between 1,250 m and 1,750 m depth, and is

identifiable by a pronounced DIP maximum centered at 1,500 m depth (~ 2.25 μmol L^{-1}) (Figure 1C). Antarctic Intermediate Water is formed by subduction between the Polar Front and the Subantarctic Zone in the ACC (Sloyan and Rintoul, 2001), while UCDW is produced by isopycnal and diapycnal mixing of Indian Ocean Deep Water with Pacific Deep Water, which spreads into the ACC zone from the north, and represents the return branch of the South Atlantic thermohaline overturning circulation (McDonagh and King, 2005; Morozov *et al.*, 2010).

Water masses of the deep ocean were identified visually and by the eOMP analysis as North Atlantic Deep Water (NADW) and Antarctic Bottom Water (AABW) which include Weddell Sea Deep Water (WSDW) (Figure 1B and supp. Figure S1). North Atlantic Deep Water is found between 1,750 m and 3,000 m depth and was observed over the entire 40°S section. North Atlantic Deep Water was identified by its salinity maximum of >34.75 PSU and DIP minimum of <2.1 μmol L^{-1} (Figure 1B & 1C). Younger and less modified NADW is carried southward with the Deep Western Boundary Current (DWBC (Garzoli *et al.*, 2015)), near the South American margin, as this is indicated visually by the strongly developed salinity maximum and DIP minimum (Figure 1C), and numerically by highest fractions of NADW calculated via the eOMP analysis (supp. Figure S1). North Atlantic Deep Water is composed from water masses that enter the subpolar North Atlantic through the deepest parts of the Greenland Scotland Ridge system and by convective overturn of water masses in the Labrador Sea. North Atlantic Deep Water is transported southwards predominately in the DWBC (Iudicone *et al.*, 2008; Talley *et al.*, 2011; Garzoli *et al.*, 2015). Antarctic Bottom Water is observed below 3,000 m depth and contained the coldest (<1°C) and most nutrient-rich waters (DIP > 2.3 μmol L^{-1}) along the section (Figure 1C). Antarctic Bottom Water is formed at several locations over the Antarctic slope (e.g., the Weddell Sea – Weddell Sea Deep Water (WSDW (Orsi *et al.*, 1999)), the Ross Sea, and the

232 Cooperation Sea), and is a mixture of Antarctic Shelf Water with Circumpolar Deep Water (Orsi
233 et al. 1999) and NADW (Siedler et al. 2001). Weddell Sea Deep Water, part of AABW, is
234 positioned below 3,500 m depth and is restricted to the abyssal planes of the Argentine Basin.
235
236 *3.2 Distribution of DPb and LpPb in the water column*
237 Dissolved Pb concentrations in the surface waters ranged from 8 to 29 pmol L^{-1}, with
238 average concentrations of 12 ± 2 (1 s.d.) pmol L^{-1} (n = 85) for the subtropical and subantarctic
239 surface waters (STSW & SASW) (Figure 2A & 4). Elevated DPb values (23 ± 3 pmol L^{-1} (n =
240 22)) were found in the upper 500 m at St. 1 – 4 near the South African margin (i.e., the Agulhas
241 Current). Slightly less elevated DPb concentrations (18 ± 3 pmol L^{-1} (n = 14)) were found near
242 the South American margin, coinciding with the position of the Brazil Current at roughly 52°W
243 (St. 20 & 21). At station 24, on the South American shelf, DPb concentrations decreased with
244 depth from 9 pmol L^{-1} at 18 m, to 5 pmol L^{-1} near the seafloor at 52 m depth (Figure 3A & S2). In
245 addition, a subsurface filament of low DPb concentrations extended from the shelf to circa 100
246 km offshore (St. 24 & 23) (supp. Figure S2). Below the upper 400 m of the water column, DPb
247 concentrations decreased with depth and produced a subsurface maximum (12 ± 1 pmol L^{-1} (n =
248 30)) in the Argentine Basin (St. 12 – 22) between 1,750 m and 3,000 m depth, coinciding with
249 the spread of NADW. The deep DPb maximum is not well reproduced by the ODV plot in Figure
250 2, but can be clearly recognized in the supp. Figure S4 and the box-whiskers-plot in Figure 4.
251 Below 3000 m depth, DPb concentrations decreased, with average concentrations of 5 ± 1 pmol
252 L^{-1} (n = 26) and 6 ± 1 pmol L^{-1} (n = 22) near the seafloor at 5,500 m depth in the center of the
253 Argentine and Cape Basins, respectively. These low DPb waters correspond to WSDW and
254 AABW.

Leachable particulate Pb (LpPb) concentrations ranged from bellow the limit of detection (LOD) to 28 pmol L^{-1}. Elevated concentrations were restricted to bottom waters on the shallow South American shelf below 30 m depth (St. 24), and below 4,500 m depth in the Argentine Basin (Figures 2B & 3). At St. 24, for example, LpPb increased with depth from 4 pmol L^{-1} at 18 m depth, to 28 pmol L^{-1} at 52 m depth (Figure 3A). At the remaining sites in the water column, LpPb concentrations stayed uniformly low, ranging from <LOD to 5 pmol L^{-1}.

Dissolved Pb concentrations measured for the crossover station shared with GA02 (40.0°S, 42.4°W) are in good agreement with the results from the earlier section (Schlitzer *et al.*, 2018) (supp. Figure S5). In contrast, DPb concentrations measured for the crossover station shared with GIPY04 (36.4°S, 13.1°E) are significantly lower (Schlitzer *et al.*, 2018), but very similar to DPb concentrations from discrete Pb isotope samples collected during D357/JC068 (supp. Figure S5). The isotope-derived data was provided by Maxence Paul, Tina van de Flierth and Mark Rehkamper (Imperial College London). Elevated DPb concentrations of up to 29 pmol L^{-1} detected near the South African continental margin in the Agulhas current are in good agreement with literature values from the same location (28 pmol L^{-1} (Helmers and van der Loeff, 1993); 29 pmol L^{-1} (Paul *et al.*, 2015)). Leachable particulate Pb concentrations of the present study are substantially lower than recent literature values from the Celtic Sea (~10 – 550 pmol L^{-1} (Rusiecka *et al.*, 2018)).

4. Discussion

4.1 Pb_{min} vs. Pb_{anth}: What fraction dominates the DPb pool in the South Atlantic surface ocean?

Recent studies have reported DPb concentrations in the Atlantic surface ocean averaging roughly 40 pmol L^{-1} in the Celtic Sea (Rusiecka *et al.*, 2018), 20 pmol L^{-1} in the (sub-)tropical

and mid-latitudinal North Atlantic (Noble *et al.*, 2015; Bridgestock *et al.*, 2016; Zurbrick *et al.*, 2018), and about 15 pmol L^{-1} in the Southeast Atlantic (Paul *et al.*, 2015). Data we have presented here show that DPb concentrations in the South Atlantic surface ocean, at 12 ± 2 pmol DPb L^{-1} (n = 85) are consistently lower than in the North Atlantic (Noble *et al.*, 2015; Bridgestock *et al.*, 2016; Bridgestock *et al.*, 2018; Rusiecka *et al.*, 2018), but similar to values from the Southeast Atlantic (Paul *et al.*, 2015) and other Southern Hemisphere oceans, like the South Pacific and Southern Ocean (10 – 15 pmol L^{-1}) (GP13, GP16, and GIPY06 (Schlitzer *et al.*, 2018)). Recent measurements of Pb isotopes suggest that 50 to 98% of the DPb in the present day northern hemisphere surface ocean still originates from anthropogenic sources (Bridgestock *et al.*, 2016). However, the extent to which DPb in the South Atlantic is anthropogenic versus mineral in origin remains unknown.

To determine whether anthropogenic or mineral Pb (Pb_{anth} and Pb_{min}, respectively) is dominating the present DPb pool in the South Atlantic surface ocean, we estimated Pb_{min} through a set of calculations, using past and present dust deposition data. First we estimated the amount of mineral and anthropogenic Pb in airborne particles from the Southern Hemisphere, using the ratio (R_{Pb}) of present and pre-industrial atmospheric Pb fluxes (Eq. 1).

$$R_{Pb} = \delta Pb_{present}/\delta Pb_{pre\text{-}ind} \quad \text{(Eq. 1)}$$

We calculated R_{Pb} for a set of 16 Antarctic ice core archives from the literature (McConnell *et al.*, 2014). McConnell *et al.* (2014), for example, reported that atmospheric Pb fluxes to Antarctica increased from 1.0 nmol m^{-2} y^{-1} in the 1850s (equals our $\delta Pb_{pre\text{-}ind}$) to 3.0 nmol m^{-2} y^{-1} in the 1920s and 3.5 nmol m^{-2} y^{-1} in the 1970s, the time of peak anthropogenic Pb emissions. Since the 1970s, atmospheric Pb fluxes to Antarctica have dropped gradually to present day values of 2.4 nmol m^{-2} y^{-1} (equals our $\delta Pb_{present}$). Using these data yields a R_{Pb} ratio of 2.4, suggesting that

present Pb fluxes to Antarctica are 2.4 times greater than they were 160 years ago and that 42% of present day atmospheric Pb fluxes to Antarctica are mineral Pb (~1.0 nmol m^{-2} y^{-1}), and 58% are anthropogenic in nature (~1.4 nmol m^{-2} y^{-1}). Another Pb dataset from a glacier in the Bolivian Andes yield a similar R_{Pb} ratio of 2.5 between the 1870s and 2010 (Eichler *et al.*, 2015), suggesting that present atmospheric Pb fluxes are similarly elevated throughout other parts of the southern hemisphere.

We then calculated the concentration of Pb_{min} by dividing 12 ± 2 pmol L^{-1} (the average DPb concentration of surface waters in this study) by R_{Pb} (Eq. 2), assuming that the DPb of the surface ocean is in equilibrium with that of the atmosphere.

$$Pb_{min} = DPb/R_{Pb} \quad \text{(Eq. 2)}$$

This new approach yields a concentration of Pb_{min} of 5 ± 1 pmol L^{-1} (42% of the DPb pool). Based on the relationship DPb = Pb_{anth} + Pb_{min}, we estimated Pb_{anth} to be 7 ± 1 pmol L^{-1}. Some simplifications had to be made for the Pb_{min} estimate: Due to a current lack of data, our approach neglects the fractional solubility of Pb_{min} and Pb_{anth} particles (Hsu *et al.*, 2005), creating an unknown degree of uncertainty. Therefore, our result for Pb_{min} and Pb_{anth} should be taken cautiously and seen in context with other available data.

The abundance of Pb_{min} in percent in our study region (42%) falls within the 2 – 50% range reported for the North Atlantic (Bridgestock *et al.*, 2016). In addition, the isotopic Pb ratio for surface waters of the Southeast Atlantic, west of the Agulhas Current ($^{206}Pb/^{207}Pb$: ~ 1.165 (Paul *et al.*, 2015)), is similar to that of the anthropogenically dominated North Atlantic ($^{206}Pb/^{207}Pb$: 1.16 – 1.17 (Bridgestock *et al.*, 2016; Bridgestock *et al.*, 2018)), which confirms that a considerable amount of surface DPb (<50%) in the Southeast Atlantic originates from anthropogenic sources. Pre-industrial dissolved Pb (DPb_{pre}) concentrations reconstructed from

banded corals from the Southern Hemisphere may represent another chance to examine the accuracy of our estimates. We are unaware of any tropical banded coral records from the South Atlantic and unfortunately, coral records from the South Pacific and the Indian Ocean appear to be contaminated by anthropogenic Pb (e.g.: Mauritius: 25 to 29 pmol L^{-1} (Shen and Boyle, 1987); Sumatra: 11 to 14 pmol L^{-1} (Lee *et al.*, 2014); Fiji, Galapagos, and Tutuila: 16 to 50 pmol L^{-1} (Shen and Boyle, 1987)). Tropical banded corals older than the ones presented in the literature (oldest bands from the 1920s and the 1970s), are required to obtain reliable levels for DPb_{pre}.

4.2 Supply and removal routes of DPb in the South Atlantic

The majority of the DPb in the ocean environment has been supplied originally by dry and wet deposition of airborne particles (Bridgestock *et al.*, 2016; Zurbrick *et al.*, 2017; Zurbrick *et al.*, 2018), or by release from suspended particulate matter (Noble *et al.*, 2015; Chien *et al.*, 2017; Rusiecka *et al.*, 2018; Schlosser, submitted to GRL). In contrast, scavenging onto the surfaces of suspended particles is the dominant DPb removal mechanism (Luengen *et al.*, 2007; Bridgestock *et al.*, 2016). In the following paragraphs we will discuss the supply and removal processes that account for the 40°S South Atlantic transect and compare them to known findings.

4.2.1 Aeolian Pb supply and residence time estimates

Aerosol deposition fluxes determined during cruise D357 in the Southeast Atlantic using rain water collectors (Chance *et al.*, 2015), and average climatology precipitation data, yields an average wet deposition flux for soluble Pb of 14 ± 12 nmol Pb m^{-2} d^{-1}. This is two orders of magnitude higher than the dry deposition of Pb of 0.09 ± 0.50 nmol Pb m^{-2} d^{-1} determined by high volume aerosol collectors and calculated by applying a deposition velocity of V_d = 0.3 cm s^{-1} (Chance *et al.*, 2015), suggesting that wet deposition of aeolian particles represents the dominant

Pb source to the South Atlantic. This is in agreement with the general notion that wet deposition is the main supply route of airborne particles and trace metals to surface waters of the open ocean (Huneeus *et al.*, 2011; Schlosser *et al.*, 2014). In addition, bulk deposition fluxes to the South Atlantic are similar in range to aerosol Pb fluxes found in other remote regions, like the Arctic Ocean, of roughly 1 nmol m^{-2} d^{-1} (Marsay *et al.*, 2018), but are higher than Pb fluxes to the Antarctic continent (~0.005 nmol Pb m^{-2} d^{-1} (McConnell *et al.*, 2014)).

We also determined an average residence time for DPb in surface waters by dividing the average depth integrated content of DPb in the surface mixed layer (494 ± 98 nmol m^{-2} in the upper 44 ± 8 m (criterion: sigma-theta = 0.125 (Kara *et al.*, 2003))), by the supply of soluble Pb due to wet deposition (14 ± 12 nmol Pb m^{-2} d^{-1} (Chance *et al.*, 2015)). We then estimated an average residence time for DPb in surface waters of 35 ± 31 days (i.e. 0 to 2 months). Our estimate is similar to the literature value from Bridgestock *et al.* (2016) who suggested a DPb residence time of 2 to 3 months for surface waters of the tropical and subtropical North Atlantic. In addition, a study from the North Pacific gyre and the North Atlantic refer to a DPb residence time in the range of 1.5 to 2.5 months using the isotopic disequilibrium of $^{210}Po/^{210}Pb$ (Chai and Urban, 2004). In any case, the residence time of DPb in the surface ocean along the transect must be short enough to allow for the inter-annual variability of DPb such as observed at the BATS time series station (Veron Alain *et al.*, 1993), but also long enough to allow spatially confined wet deposition events to be averaged to produce the observed uniform distribution in the surface ocean along the 40°S transect.

4.2.2 Riverine input

On the South American shelf, a gradually decreasing zonal freshwater lens (28 – 34 PSU) is clearly visible within the top 20 m of the water column, extending from the shelf to ca. 150 km

offshore (supp. Figure S2), indicative of the mixing of freshwater from the Rio de la Plata with the surrounding seawater and zonal water mass transport following the South Atlantic Current. However, DPb concentrations within the freshwater lens are very low (varying from 7 to 9 pmol L^{-1}; supp. Figure S2), suggesting that the freshwater from the Rio de la Plata river did not deliver large quantities of DPb into the South Atlantic. This finding is in good agreement with previous studies (Steding *et al.*, 2000; Qian *et al.*, 2015) that suggested that during the transition from riverine freshwater to seawater, DPb concentrations are diminished from a brackish water body by sorption of DPb onto surfaces of freshly precipitated particles, with subsequent accumulation of LpPb in the suspended particle pool and underlying sediments (Roussiez *et al.*, 2011; Chuang *et al.*, 2014; Bastami *et al.*, 2015).

4.2.3 Pb scavenging onto particle surfaces

It is generally agreed that scavenging onto the surfaces of suspended particles represents the main removal mechanism for DPb from seawater (Helmers and van der Loeff, 1993; Chuang *et al.*, 2014; Yang *et al.*, 2015). We found evidence that this process is also taking place in the South Atlantic.

At all sampling sites in the Argentine Basin, including St. 24 (Figure 3A) on the shallow shelf, and also the offshore St. 20 (Figure 3B), DPb concentrations decreased with increasing proximity to the seafloor, while LpPb concentrations concurrently increased, reaching highest concentrations close to the seafloor. At St. 20 below 4400 depth, DPb concentrations remained the same (9.3 ± 0.4 pmol L^{-1} ($n = 3$)). In addition, elevated LpPb and reduced DPb concentrations coincided with elevated turbidity, as indicated by the reduced transmittance in the nepheloid layer near the seafloor (Figure 3A and 3B), supporting the notion that the sorption onto resuspended sediment particles removed DPb from South Atlantic bottom waters. As indicated by the

393 transmissometer data, these nepheloid layers in the deep ocean (Richardson *et al.*, 1993) extended
394 up to 250 m above the seafloor (Figure 3B) and were restricted to the Argentine Basin (i.e., they
395 were not observed in the Cape Basin) (Figures 1B & 2B). However, it has been well documented
396 that tidal waves, strong currents, and storm events can stimulate the formation of nepheloid layers
397 in the deep sea (Noble *et al.*, 2015), along continental margins (Rusiecka *et al.*, 2018), on
398 continental shelf zones (Chien *et al.*, 2017), and in riverine dominated coastal areas (Ferrari and
399 Ferrario, 1989).

400 We assume that in addition to the particle abundance, the composition and/or size of the
401 particles could play a critical role in explaining the scavenging capacity of DPb onto particle
402 surfaces. Apart from St. 24 on the shelf, DPb and LpPb from the nepheloid layers in the
403 Argentine Basin follow a negative linear regression with a similar slope of circa -0.35 ± 0.3, n =
404 22, $R^2 \approx 0.41$ (Figure 3C; average slope 1: -0.38 and slope 3: -0.32), indicating that the removal
405 of DPb is related to the abundance of resuspended particles. However, samples from St. 24 (the
406 only station on the shallow shelf) describe a negative linear regression different to the other
407 stations, with the slope of -0.15 ($R^2 = 0.85$) being slightly less steep, suggesting that DPb was
408 less efficiently removed from bottom waters on the shelf. A possible explanation might be change
409 in particle size (Rusiecka et al., 2018), and/or a change in composition of the particulate pool
410 (Balistrieri *et al.*, 1981), however, since it is data from just a single station (three data points), the
411 results should be interpreted very restrictively.

412 Recent observations in the North Atlantic and Philippian Sea indicate a possible sedimentary
413 source of DPb (Noble *et al.*, 2015; Chien *et al.*, 2017), suggesting that there is a dynamic
414 equilibrium between DPb and suspended particulate Pb (Rusiecka *et al.*, 2018). Based on ^{224}Ra
415 measurements and a positive linear regression between DPb and LpPd (both species increase),

Rusiecka *et al.* (2018), for instance concluded that DPb is released from suspended sediments that are strongly enriched in Pb, leading to an accumulation of both DPb and LpPb in bottom waters of the Celtic Sea. Whilst being in contradiction to the findings of the present study, the observation of Rusiecka *et al.* (2018) and others might be explained by the size of the available reservoir of sedimentary Pb. While sediments in Northern Hemisphere oceans received larger amounts of mineral and anthropogenic Pb by atmospheric deposition (up to 80 µg Pb g^{-1} in shelf sediments at the Iberian peninsula, North Atlantic (Mil-Homens *et al.*, 2016)), sediments in the Southern Hemisphere received less Pb_{min} and Pb_{anth} (roughly 3 µg Pb g^{-1} in shelf sediments off the west coast of Chile, South Pacific (Chandía and Salamanca, 2012)), indicating a less pronounced reservoir of sedimentary Pb in Southern Hemisphere oceans.

4.3 Tracing water masses using DPb

Concentrations of DPb indicate the recent supply of mineral and anthropogenic Pb to the surface ocean (Bridgestock *et al.*, 2016; Bridgestock *et al.*, 2018). Lead removal processes, such as scavenging and water mass mixing will reduce DPb concentrations (Helmers and van der Loeff, 1993; Luengen *et al.*, 2007; Chuang *et al.*, 2014), lowering initially elevated DPb concentrations in water masses slowly with time when the atmospheric supply is reduced or stopped (Yang *et al.*, 2015). However, elevated DPb concentrations may persist for a period of time. This has been shown to be the case for NADW and MOW (IDP 2017; section GA02 & GA03 (Noble *et al.*, 2015; Schlitzer *et al.*, 2018; Zurbrick *et al.*, 2018)), meaning that the residence time of DPb in waters situated below the surface layer (or in other waters with low particle abundance) is generally longer (up to 100 years (Nozaki, 1986)) than in surface waters and that DPb can be available for some period of time, following addition, as a water mass tracer.

We identified four surface and five deep water masses along the 40°S section, using temperature, salinity, and nutrient data both visually (Figure 1) and resolved their respective contributions in water mass fractions numerically using extended Optimum MultiParameter (eOMP) analysis (supp. Figure S1)). Even though individual DPb concentrations are difficult to recognize for the nine water masses in the ODV plot of Figure 2, box plot statistics indicate that almost all of these water masses have a distinct DPb concentration (Figure 4). We assessed the water masses by their DIP and salinity characteristics and applied the DPb concentrations from each water mass to the box plot statistics. Median, first quartile, and third quartile for each water mass are listed in Table 2.

4.3.1 Surface water masses

Subtropical (STSW) and the subantarctic (SASW) surface waters are limited to the upper 400 to 500 m of the water column and differ greatly by temperature, salinity, and nutrient content (Figure 1). Despite both water masses being separated by a biogeochemical divide (the STF) (Figure 1), DPb concentrations are similar (12 ± 2 pmol DPb L^{-1}; Figure 4). We can therefore assume that the combined magnitude of supply and removal processes created the uniform distribution of DPb in these otherwise very different water masses.

In contrast to open ocean sites, two DPb hot-spots were found near the continental margins: (i) offshore of the South American margin, within the warm and salty Brazil Current (BC: 18 ± 3 pmol L^{-1} (n = 14)), and (ii) within the warm but less salty Agulhas Current (AC ~ 23 ± 3 pmol L^{-1} (n = 22)) near the South African margin (Figures 2 & 4). Whilst it is already known that the Agulhas Current is heavily loaded with Pb_{anth}, carrying the supply signal from three distinct endmembers; (a) from the Agulhas Current source region in the Indian Ocean, (b) from South African coastal waters, and (c) from the offshore South Atlantic ocean (Echegoyen *et al.*, 2014;

462 Paul *et al.*, 2015), elevated DPb levels in the Brazil Current have not been reported before. We
463 assume that similar to the Agulhas Current, elevated DPb concentrations in the Brazil Current
464 originate from the tropical source region of the current at about 10°S (20 ± 3 pmol L^{-1} (n = 21)
465 (Bridgestock *et al.*, 2016)), and from Pb supplied by the atmosphere during the passage along the
466 South American coast. However, the contribution of the different Pb sources to the Brazil Current
467 at 40°S remains unknown.

468 *4.3.2 Intermediate water masses*

469 Dissolved Pb concentrations gradually decrease from roughly 12 pmol L^{-1} at the base of the
470 surface ocean to circa 10 pmol L^{-1} at 1,750 m depth (Figure 4 & S4), which corresponds to the
471 part of the water column we identified as AAIW and UCDW. Median DPb concentrations for
472 AAIW of 11 ± 1 pmol L^{-1} are insignificantly higher than for UCDW (10 ± 1 pmol L^{-1}). The DPb
473 concentrations within the two water masses are not statistically different from another.
474 Nevertheless, we assume that the shallow depth of both water masses and the interplay of
475 atmospheric deposition, vertical mixing, and surface scavenging modified the characteristic DPb
476 concentration of UCDW and AAIW as the water masses were transported from their source
477 regions to 40°S (McDonagh and King, 2005; Morozov *et al.*, 2010).

478 *4.3.3 The North Atlantic Deep Water*

479 While DPb concentrations in the water column of the Cape Basin (St. 1 – St. 11) gradually
480 decreased with depth below 500 m, hence showing no clear indication for elevated DPb levels in
481 the deeper ocean (NADW-e = 8 ± 1 pmol L^{-1} (n = 21)), by contrast, the DPb in the Argentine
482 Basin (St. 12 – St. 22) had a visible subsurface maximum (NADW-w = 12 ± 1 pmol L^{-1} (n = 30))
483 that decreased from west to east and coincided with the spread of NADW (Figures 4, S1 & S4).

484 North Atlantic Deep Water is located between 1,750 m and 3,000 m depth and stretches over
485 the entire 40°S transect, as illustrated by its salinity maximum, DIP minimum, and our results
486 from the eOMP analysis (Figures 1 and S1). The salinity maximum gradually decreased from
487 west to east (as DIP increased), from a fully pronounced salinity (and DPb) maximum near the
488 South American margin (St. 20 and 21; 34.92 psu) to a more spread out and less pronounced
489 maximum in the Eastern Cape Basin (St. 1 – 11; 34.77 psu; supp. Figure S4), suggesting
490 differences in diapycnal mixing (the vertical diffusive component) between both basins.
491 Assuming that the turbulent and diffusive mixing at 2,500 m (the depth of NADW), away from
492 continental margins and seamounts, is similar to the mean world ocean background values
493 (Kunze *et al.*, 2006; Marzeion *et al.*, 2007; Banyte *et al.*, 2012). The decrease of the salinity
494 maximum (from west to east) must be then related to the dwell time of NADW in the ocean
495 interior. This suggests that NADW remains less modified (diluted & mixing with neighboring
496 water masses), and is younger in the Argentine than in the Cape Basin. This is in general
497 agreement with what is understood of the oceanography of the region. Talley *et al.* (2011), for
498 example, showed that due to fewer physical barriers (e.g. Mid-Atlantic Ridge), similar isopycnal
499 layers at 2,500 m depth (NADW) extend further south in the western than in the eastern basin of
500 the South Atlantic. In addition, Garzoli *et al.* (2015) showed that NADW waters transported with
501 the Deep Western Boundary Current (DWBC) near the Brazilian margin reaches velocities of up
502 to 10 cm s^{-1}, transporting NADW waters quickly from the Equator to 40°S. In contrast, common
503 deep water velocities for the South Atlantic range from 0.2 to 0.9 cm s^{-1} (Huhn *et al.*, 2008),
504 ensuring a longer mixing time with adjacent waters.

505 Accordingly, the most pronounced salinity and DPb maxima at circa 2,500 m depth (up to 24
506 pmol DPb L^{-1} at St. 20; supp. Figure S4) coincided with the position of the DWBC, which, based

on the eOMP analysis, contained roughly 80% NADW (supp. Figure S1). Waters from the remaining sites were already more diluted and contained between 60% and 70% NADW, indicating that NADW's Pb signal at these sites has been reduced by prolonged scavenging and/or dilution with low DPb waters (UCDW & AABW). Alternatively, since the samples with lower DPb concentrations represent older NADW than the samples with higher DPb concentrations, it may be that the older NADW was exposed to the atmosphere at a time when Pb emissions were lower (Zurbrick et al., 2018).

4.3.4 The Bottom Waters

Lowest DPb concentrations (<7 pmol L^{-1}) from this study were detected below 3,000 m depth in AABW and WSDW. Although AABW is composed from WSDW we chose to distinguish the two along the section because very different blends of AABW can be seen on the section and related to the topographic control on the AABW spreading with very old AABW east and younger AABW west of the Mid Atlantic Ridge (Johnson 2008). The WSDW is restricted to the abyssal plain of the Argentine Basin and contained insignificantly lower amounts of DPb (5.0 ± 1.1 pmol L^{-1}) than did AABW (6.0 ± 1.2 pmol L^{-1}) (Figure 4 & S1). The differences are not statistically significant, implying that the source region of WSDW and the remaining AABW forming sites (e.g., Ross Sea, Cooperation Sea) received similar amounts of airborne Pb. To what extent other Pb sources, such as glacial melt (Ndungu *et al.*, 2016), influence the Pb supply in both source regions remains unknown.

4.3.5 Modeling the distribution of DPb

Based on the estimated amounts of AAIW, NADW, and WSDW in the water column (determined by the eOMP analysis (Figure S1)), the amount of DPb in the water column was

numerically reconstructed using a fairly simple model (Figure 5). Together with the median DPb contents of AAIW (10.8 pmol L^{-1}), NADW w. (12.0 pmol L^{-1}) and WSDW (5.0 pmol L^{-1}) (listed in Table 2), the ratio of AAIW, NADW, and WSDW in the water column were used to model the expected DPb concentrations. Thus, the modeled content of DPb reflects the mixing of NADW with AAIW and WSDW. Due to the limited applicability of the eOMP analysis in the surface ocean (e.g., nutrient uptake, atmospheric gas exchange), modeled DPb values are restricted to waters below 500 m depth.

The modeling results in Figure 5 compare well with the measured distribution of DPb in Figure 2A, reproducing the elevated DPb levels in NADW-w (DWBC) and the reduced DPb levels in WSDW (AABW). The residual between measured and modeled values ranges generally between +2 and -2 pmol L^{-1}, suggesting that below 500 m depth, the DPb content in NADW and adjacent water masses is mainly controlled by water mass mixing. Moreover, other processes, such as Pb scavenging and vertical export, which considerably effect the DPb distribution in the surface ocean (Luengen et al. 2007), are only marginally involved in the spreading of DPb in the deep sea.

Although all deeper water masses (below 500m) along the JC086 section originate from regions upstream of the section (north and south) it still is reasonable to assume that the water mass composition along the section is the result of a mixture of endmember found at selected locations along the section (García-Ibáñez *et al.,* 2018). Therefore we derived all source water definitions from JC086 observations (Table 2), guided by extrema in T/S characteristics. The in general low mass residuals of the eOMP analysis (Figure 5) confirm our assumption on the water mass definitions. The appearance of increased mass residuals in the eastern part of the section in the NADW depth range indicate Central Deep Water from the Indian Ocean sector of the

553 Southern Ocean may have contributed to the water mass composition. However, the still low
554 mass residuals (<4%) indicate a weak impact on the results presented here.
555
556 **5. Conclusion**
557 The ongoing effort to reduce the emission of Pb from coal fired power plants, ore
558 smelters, and other anthropogenic sources to the environment has resulted in a continuous
559 reduction of DPb concentrations in most parts of the Atlantic surface ocean. Nonetheless, present
560 day dissolved Pb concentrations of the South Atlantic remain notably higher than preindustrial
561 levels, with 58% of the DPb in these waters originating from anthropogenic sources. Continuing
562 efforts in environmental regulations of Pb emissions would be necessary to achieve DPb
563 concentrations as low as our estimate of 5 pmol L^{-1} in the preindustrial South Atlantic surface
564 ocean.
565 It appears that to a limited degree, DPb can be used to trace water masses in the ocean
566 interior. At the moment, subsurface water masses like AAIW, NADW, and AABW, and surface
567 currents like the Agulhas and Brazil Current are sufficiently distinct in their DPb content for DPb
568 to be useful as a tracer in the Atlantic Ocean. As our results show, the DPb content in the ocean
569 interior is mainly controlled by the mixing of water masses, which suggests that the distribution
570 of DPb below the upper 500 m can be estimated by (i) the ratio of the water masses and (ii) the
571 Pb-signature of these waters at their source regions. Over the coming decades, however,
572 thermohaline overturning circulation, internal mixing, will blend DPb signals of individual water
573 masses, homogenizing the DPb content of the subsurface ocean, and perhaps obliterating the
574 perturbation that is anthropogenically-sourced Pb.
575

Acknowledgement

We would like to thank captain and crew of RRS *Discovery* and RRS *James Cook*. In addition, we thank chief scientist Gideon Henderson, the other participants of both cruises, especially the CTD deployment and sampling party, Maeve Lohan and Angie Milne, and the two independent reviewers. The work was supported by NERC funding NE/H004394/1.

References

Akumu, J., 2019. Overview of Progress made to Introduce Cleaner Fuels and Vehicles: 2016 to 2019. UN environment: The 12th Global Partners Meeting of the Partnership for clean Fuels and Vehicles, Paris, France

Balistrieri, L., Brewer, P.G., Murray, J.W., 1981. Scavenging residence times of trace metals and surface chemistry of sinking particles in the deep ocean. Deep Sea Research Part A. Oceanographic Research Papers 28 (2), 101-121.

Banyte, D., Tanhua, T., Visbeck, M., Wallace, D.W.R., Karstensen, J., Krahmann, G., Schneider, A., Stramma, L., Dengler, M., 2012. Diapycnal diffusivity at the upper boundary of the tropical North Atlantic oxygen minimum zone. Journal of Geophysical Research: Oceans 117 (C9).

Bastami, K.D., Neyestani, M.R., Shemirani, F., Soltani, F., Haghparast, S., Akbari, A., 2015. Heavy metal pollution assessment in relation to sediment properties in the coastal sediments of the southern Caspian Sea. Marine Pollution Bulletin 92 (1-2), 237–243.

Boyle, E.A., Lee, J.-M., Echegoyen-Sanz, Y., Noble, A.E., Moos, S., Carrasco, G.G., Zhao, N., Kayser, R.A., Zhang, J.Z., Gamo, T., Obata, H., Norisuye, K., 2014. Anthropogenic Lead Emissions in the Ocean: The Evolving Global Experiment Oceanography 27 (1), 69-75.

598 Bridgestock, L., Rehkämper, M., van de Flierdt, T., Paul, M., Milne, A., Lohan, M.C.,
599 Achterberg, E.P., 2018. The distribution of lead concentrations and isotope compositions in the
600 eastern Tropical Atlantic Ocean. Geochimica et Cosmochimica Acta 225, 36-51.
601 Bridgestock, L., van de Flierdt, T., Rehkamper, M., Paul, M., Middag, R., Milne, A., Lohan,
602 M.C., Baker, A.R., Chance, R., Khondoker, R., Strekopytov, S., Humphreys-Williams, E.,
603 Achterberg, E.P., Rijkenberg, M.J.A., Gerringa, L.J.A., de Baar, H.J.W., 2016. Return of
604 naturally sourced Pb to Atlantic surface waters. Nature Communication 7, 1-12.
605 Chai, Y., Urban, N.R., 2004. 210Po and 210Pb distributions and residence times in the nearshore
606 region of Lake Superior. Journal of Geophysical Research: Oceans 109 (C10).
607 Chance, R., Jickells, T.D., Baker, A.R., 2015. Atmospheric trace metal concentrations, solubility
608 and deposition fluxes in remote marine air over the south-east Atlantic. Marine Chemistry 177,
609 45-55.
610 Chandía, C., Salamanca, M., 2012. Long-term monitoring of heavy metals in Chilean coastal
611 sediments in the eastern South Pacific Ocean. Marine Pollution Bulletin 64, 2254-2260.
612 Chen, M., Goodkin, N F., Boyle, E. A., Switzer, A. D., Bolton, A., 2016. Lead in the the western
613 South China Sea: Evidence of atmospheric depsoition and upwelling. Geophysical Research
614 Letters 43, 4490-4499.
615 Chien, C.T., Ho, T.Y., Sanborn, M.E., Yin, Q.Z., Paytan, A., 2017. Lead concentrations and
616 isotopic compositions in the Western Philippine Sea. Marine Chemistry 189 (10-16).
617 Chuang, C.Y., Santschi, P.H., Jiang, Y.L., Ho, Y.F., Quigg, A., Guo, L.D., Ayranov, M.,
618 Schumann, D., 2014. Important role of biomolecules from diatoms in the scavenging of particle-
619 reactive radionuclides of thorium, protactinium, lead, polonium, and beryllium in the ocean: A
620 case study with Phaeodactylum tricornutum. Limnology and Oceanography 59 (4), 1256-1266.

621 Cziczo, D.J., Stetzer, O., Worringen, A., Ebert, M., Weinbruch, S., Kamphus, M., Gallavardin,
622 S.J., Curtius, J., Borrmann, S., Froyd, K.D., Mertes, S., Mohler, O., Lohmann, U., 2009.
623 Inadvertent climate modification due to anthropogenic lead. Nature Geosci 2 (5), 333-336.
624 Damle, A.S., Ensor, D.S., Ranade, M.B., 1981. Coal Combustion Aerosol Formation
625 Mechanisms: A Review. Aerosol Science and Technology 1 (1), 119-133.
626 Echegoyen, Y., Boyle, E.A., Lee, J.-M., Gamo, T., Obata, H., Norisuye, K., 2014. Recent
627 distribution of lead in the Indian Ocean reflects the impact of regional emissions. Proceedings of
628 the National Academy of Sciences 111 (43), 15328-15331.
629 European Environment Agency, 2018. Air quality in Europe — 2018 report. EEA Report.
630 European Environment Agency, pp. 1-83.
631 Eichler, A., Gramlich, G., Kellerhals, T., Tobler, L., Schwikowski, M., 2015. Pb pollution from
632 leaded gasoline in South America in the context of a 2000-year metallurgical history. Science
633 advances 1 (2), e1400196-e1400196.
634 Engineering, E.H., 2011. Emission of hazardous air pollutants from coal-fired power plants.
635 Environmental Health & Engineering Report.
636 Ferrari, G.M., Ferrario, P., 1989. Behavior of Cd, Pb, and Cu in the marine deltaic area of the Po
637 River (North Adriatic Sea). Water, Air, and Soil Pollution 43 (3-4), 323-343.
638 Fine, R. A., 2011. Observations of CFCs and SF6 as Ocean Tracers. Annual Review of Marine
639 Science 3, 173-195
640 García-Ibáñez, M. I., Pérez, F. F., Lherminier, P., Zunino, P., Mercier, H., Tréguer, P., 2018.
641 Water mass distributions and transports for the 2014 GEOVIDE cruise in the North Atlantic.
642 Biogeosciences 15, 2075-2090.

643 Garzoli, S.L., Dong, S., Fine, R., Meinen, C.S., Perez, R.C., Schmid, C., van Sebille, E., Yao, Q.,
644 2015. The fate of the Deep Western Boundary Current in the South Atlantic. Deep Sea Research
645 Part I: Oceanographic Research Papers 103, 125-136.
646 Helmers, E., van der Loeff, M.M.R., 1993. Lead and Aluminum in Atlantic Surface Waters
647 (50°N to 50°S) Reflecting Anthropogenic and Natural Sources in the Eolian Transport. Journal of
648 Geophysical Research 98 (C11), 20261-20273.
649 Hsu, S.-C., Lin, F.-J., Jeng, W.-L., 2005. Seawater solubilityof natural and anthropogenic metals
650 within ambient aerosols collected from Taiwan coastal sites. Atmospheric Environment 39, 3989-
651 4001.
652 Huhn, O., Roether, W., Steinfeldt, R., 2008. Age spectra in North Atlantic Deep Water along the
653 South American continental slope, 10°N–30°S, based on tracer observations. Deep Sea Research
654 Part I: Oceanographic Research Papers 55 (10), 1252-1276.
655 Huneeus, N., Schulz, M., Balkanski, Y., Griesfeller, J., Prospero, J., Kinne, S., Bauer, S.,
656 Boucher, O., Chin, M., Dentener, F., Diehl, T., Easter, R., Fillmore, D., Ghan, S., Ginoux, P.,
657 Grini, A., Horowitz, L., Koch, D., Krol, M.C., Landing, W., Liu, X., Mahowald, N., Miller, R.,
658 Morcrette, J.J., Myhre, G., Penner, J., Perlwitz, J., Stier, P., Takemura, T., Zender, C.S., 2011.
659 Global dust model intercomparison in AeroCom phase I. Atmospheric Chemistry and Physics 11
660 (15), 7781-7816.
661 Hydes, D.J., Aoyama, M., Aminot, A., Bakker, K., Becker, S., Coverly, S., Daniel, A., Dickson,
662 A.G., Grosso, O., Kerouel, R., van Ooijen, J., Sato, K., Tanhua, T., Woodward, E.M.S., Zhang,
663 J.Z., 2010. Detrmination of dissolved nutrients (N, P, Si) in seawater with high precision and
664 inter-comparability using gas-segment continous flow analyzer

GO-Ship repeat hydrography manual: A collection of expert reports and guidlines. IOCCP Report No. 14, ICPO Publication Series No. 134, Version 1.

Iudicone, D., Speich, S., Madec, G., Blanke, B., 2008. The Global Conveyor Belt from a Southern Ocean Perspective. Journal of Physical Oceanography 38 (7), 1401-1425.

Kagaya, S., Maebe, E., Inoue, Y., Kamichatani, W., Kajiwara, T., Yanai, H., Saito, M., Tohda, K., 2009. A solid phase extraction using a chelate resin immobilizing carboxymethylated pentaethylenehexamine for separation and preconcentration of trace elements in water samples. Talanta 79, 146-152.

Kara, A.B., Rochford, P.A., Hurlburt, H.E., 2003. Mixed layer depth variability over the global ocean. Journal of Geophysical Research: Oceans 108 (C3).

Kelly, A.E., Reuer, M.K., Goodkin, N.F., Boyle, E.A., 2009. Lead concentrations and isotopes in corals and water near Bermuda. Earth and Planetary Science Letters 283, 93-100.

Krause, P., Kriews, M., Dannecker, W., Garbe-Schönberg, C.-D., Kersten, M., 1993. Determination of 2°6/2°7pb isotope ratios by ICP-MS in particulate matter from the North Sea environment. Fresenius J. Anal. Chem. 347, 324-329.

Kunze, E., Firing, E., Hummon, J.M., Chereskin, T.K., Thurnherr, A.M., 2006. Global Abyssal Mixing Inferred from Lowered ADCP Shear and CTD Strain Profiles. Journal of Physical Oceanography 36 (8), 1553-1576.

Lee, J.-M., Boyle, E.A., Gamo, T., Obata, H., Norisuye, K., Echegoyen, Y., 2015. Impact of anthropogenic Pb and ocean circulation on the recent distribution of Pb isotopes in the Indian Ocean. Geochimica et Cosmochimica Acta 170, 126-144.

686 Lee, J.-M., Boyle, E.A., Suci Nurhati, I., Pfeiffer, M., Meltzner, A.J., Suwargadi, B., 2014. Coral-
687 based history of lead and lead isotopes of the surface Indian Ocean since the mid-20th century.
688 Earth and Planetary Science Letters 398, 37-47.
689 Lima, A.L., Bergquist, B.A., Boyle, E.A., Reuer, M.K., Dudas, F.A., Reddy, C., Eglinton, T.,
690 2005. High-resolution historical records from Pettaquamscutt River basin sediments: 2. Pb
691 isotopes reveal a potential new stratigraphic marker. Geochimica et Cosmochimica Acta 69 (7),
692 1813-1824.
693 Luengen, A.C., Raimondi, P.T., Flegal, A.R., 2007. Contrasting biogeochemistry of six trace
694 metals during the rise and decay of a spring phytoplankton bloom in San Francisco Bay.
695 Limnology and Oceanography 52 (3), 1112-1130.
696 Mahowald, N.M., Hamilton, D.S., Mackey, K.R.M., Moore, J.K., Baker, A.R., Scanza, R.A.,
697 Zhang, Y., 2018. Aerosol trace metal leaching and impacts on marine microorganisms. Nature
698 Communications 9 (1), 2614.
699 Marsay, C.M., Kadko, D., Landing, W.M., Morton, P.L., Summers, B.A., Buck, C.S., 2018.
700 Concentrations, provenance and flux of aerosol trace elements during US GEOTRACES Western
701 Arctic cruise GN01. Chemical Geology 502, 1-14.
702 Marzeion, B., Levermann, A., Mignot, J., 2007. The Role of Stratification-Dependent Mixing for
703 the Stability of the Atlantic Overturning in a Global Climate Model*. Journal of Physical
704 Oceanography 37, 2672-2681.
705 McCartney, M.S., 1977. Subantarctic Mode Water. Deep-Sea Research 24, 103-119.
706 McConnell, J.R., Maselli, O.J., Sigl, M., Vallelonga, P., Neumann, T., Anschütz, H., Bales, R.C.,
707 Curran, M.A.J., Das, S.B., Edwards, R., Kipfstuhl, S., Layman, L., Thomas, E.R., 2014.

708 Antarctic-wide array of high-resolution ice core records reveals pervasive lead pollution began in
709 1889 and persists today. Scientific Reports 4, 5848.
710 McDonagh, E.L., King, B.A., 2005. Oceanic Fluxes in the South Atlantic. Journal of Physical
711 Oceanography 35 (1), 109-122.
712 Mil-Homens, M., Vale, C., Naughton, F., Brito, P., Drago, T., Anes, B., Raimundo, J., Schmidt,
713 S., Caetano, M., 2016. Footprint of roman and modernmining activities in a sediment core from
714 the southwestern Iberian Atlantic shelf. Science of The Total Environment 571, 1211-1221.
715 Morozov, E.G., Demidov, A.N., Tarakanov, R.Y., Zenk, W., 2010. Deep Water Masses of the
716 South and North Atlantic. Abyssal Channels in the Atlantic Ocean. Springer Science+Business
717 Media B.V., pp. 25-50.
718 Murphy, D.M., Hudson, P.K., Cziczo, D.J., Gallavardin, S., Froyd, K.D., Johnston, M.V.,
719 Middlebrook, A.M., Reinard, M.S., Thomson, D.S., Thornberry, T., Wexler, A.S., 2007.
720 Distribution of lead in single atmospheric particles. Atmospheric Chemistry and Physics 7 (12),
721 3195-3210.
722 Ndungu, K., Zurbrick, C.M., Stammerjohn, S., Severmann, S., Sherrell, R.M., Flegal, A.R., 2016.
723 Lead Sources to the Amundsen Sea, West Antarctica. Environmental Science & Technology 50
724 (12), 6233-6239.
725 Noble, A.E., Echegoyen-Sanz, Y., Boyle, E.A., Ohnemus, D.C., Lam, P.J., Kayser, R., Reuer,
726 M., Wu, J., Smethie, W., 2015. Dynamic variability of dissolved Pb and Pb isotope composition
727 from the U.S. North Atlantic GEOTRACES transect. Deep Sea Research Part II: Topical Studies
728 in Oceanography 116, 208-225.
729 Nozaki, Y., 1986. 226Ra222Rn210Pb systematics in seawater near the bottom of the ocean. Earth
730 and Planetary Science Letters 80 (1), 36-40.

731 Orsi, A.H., Johnson, G.C., Bullister, J.L., 1999. Circulation, mixing, and production of Antarctic
732 Bottom Water. Progress in Oceanography 43 (1), 55-109.
733 Paul, M., van de Flierdt, T., Rehkämper, M., Khondoker, R., Weiss, D., Lohan, M.C., Homoky,
734 W.B., 2015. Tracing the Agulhas leakage with lead isotopes. Geophysical Research Letters 42,
735 8515-8521.
736 Qian, Y., Zhang, W., Yu, L., Feng, H., 2015. Metal Pollution in Coastal Sediments. Current
737 Pollution Reports 1 (4), 203-219.
738 Rapp, I., Schlosser, C., Rusiecka, D., Gledhill, M., Achterberg, E.P., 2017. Automated
739 preconcentration of Fe, Zn, Cu, Ni, Cd, Pb, Co, and Mn in seawater with analysis using high-
740 resolution sector field inductively-coupled plasma mass spectrometry. Analytica Chimica Acta
741 976, 1-13.
742 Richardson, M.J., Weatherly, G.L., Gardner, W.D., 1993. Benthic storms in the Argentine Basin.
743 Deep Sea Research Part II 40 (4-5), 975-987.
744 Roussiez, V., Ludwig, W., Radakovitch, O., Probst, J.-L., Monaco, A., Charrière, B., Buscail, R.,
745 2011. Fate of metals in coastal sediments of a Mediterranean flood-dominated system: An
746 approach based on total and labile fractions. Estuarine, Coastal and Shelf Science 92, 486-495.
747 Rusiecka, D., Gledhill, M., Milne, A., Achterberg, E.P., Annett, A.L., Atkinson, S., Birchill, A.,
748 Karstensen, J., Lohan, M., Mariez, C., Middag, R., Rolison, J.M., Tanhua, T., Ussher, S.,
749 Connelly, D., 2018. Anthropogenic Signatures of Lead in the Northeast Atlantic. Geophysical
750 Research Letters 45 (6), 2734-2743.
751 Schlitzer, R. et al. 2018. The GEOTRACES Intermediate Data Product 2017. Chemical Geology.
752 Schlosser, C., submitted to GRL. Mechanisms of Pb supply and removal in two remote (sub-
753)polar ocean regions

754 Schlosser, C., Klar, J.K., Wake, B.D., Snow, J.T., Honey, D.J., Woodward, E.M.S., Lohan, M.C.,
755 Achterberg, E.P., Moore, C.M., 2014. Seasonal ITCZ migration dynamically controls the location
756 of the (sub)tropical Atlantic biogeochemical divide. Proceedings of the National Academy of
757 Sciences 111 (4), 1231-1232.
758 Shen, G.T., Boyle, E.A., 1987. Lead in corals: reconstruction of historical industrial fluxes to the
759 surface ocean. Earth and Planetary Science Letters 82 (3), 289-304.
760 Sloyan, B.M., Rintoul, S.R., 2001. Circulation, Renewal, and Modification of Antarctic Mode
761 and Intermediate Water. Journal of Physical Oceanography 31, 1005-1030.
762 Steding, D.J., Dunlap, C.E., Flegal, A.R., 2000. New isotopic evidence for chronic lead
763 contamination in the San Francisco Bay estuary system: implications for the persistence of past
764 industrial lead emissions in the biosphere. Proceedings of the National Academy of Sciences 97,
765 11181–11186.
766 Stramma, L., Ikeda, Y., Peterson, R.G., 1990. Geostrophic transport in the Brazil current region
767 north of 20°S. Deep Sea Research Part A. Oceanographic Research Papers 37 (12), 1875-1886.
768 Stramma, L., Lutjeharms, J.R.E., 1997. The flow field of the subtropical gyre in the South Indian
769 Ocean into the Southeast Atlantic Ocean: a case study. Journal of Geophysical Research 99,
770 14053-14070.
771 Stramma, L., Peterson, R.G., 1990. The South Atlantic Current. Journal of Physical
772 Oceanography 20 (6), 846-859.
773 Talley, L.D., Pickard, G.L., Emery, W.J., Swift, J.H., 2011. Chapter 9 - Atlantic Ocean. In:
774 Talley, L.D., Pickard, G.L., Emery, W.J., Swift, J.H. (Eds.), Descriptive Physical Oceanography
775 (Sixth Edition). Academic Press, Boston, pp. 245-301.

776 Veron Alain, J., Church Thomas, M., Flegal, A.R., Patterson Clair, C., Erel, Y., 1993. Response
777 of lead cycling in the surface Sargasso Sea to changes in tropospheric input. Journal of
778 Geophysical Research: Oceans 98 (C10), 18269-18276.
779 Yang, W.F., Guo, L.D., Chuang, C.Y., Santschi, P.H., Schumann, D., Ayranov, M., 2015.
780 Influence of organic matter on the adsorption of Pb-210, Po-210, Be-7 and their fractionation on
781 nanoparticles in seawater. Earth and Planetary Science Letters 423, 193-201.
782 Zhang, J.-Z., Chi, J., 2002. Automated analysis of nanomolar concentrations of phosphate in
783 natural waters with liquid waveguide. Environmental Science and Technology 36 (5), 1048-1053.
784 Zurbrick, C.M., Boyle, E.A., Kayser, R., Reuer, M.K., Wu, J., Planquette, H., Shelley, R.,
785 Boutorh, J., Cheize, M., Contreira, L., Menzel Barraqueta, J.L., Sarthou, G., 2018. Dissolved Pb
786 and Pb isotopes in the North Atlantic from the GEOVIDE transect (GEOTRACES GA-01) and
787 their decadal evolution. Biogeosciences 15, 4995-5014.
788 Zurbrick, C.M., Gallon, C., Flegal, A.R., 2017. Historic and Industrial Lead within the Northwest
789 Pacific Ocean Evidenced by Lead Isotopes in Seawater. Environmental Science & Technology 51
790 (3), 1203-1212.

791
792
793
794
795
796
797
798

Data availability

The presented data is available at the British Oceanographic Data Centre (BODC) and are part of the Intermediate Data Product, IDP 2017, obtainable at the GEOTRACES website (http://www.geotraces.org/dp/idp2017).

Author contribution

CS designed the experiments and analyzed the samples from JC068 and D357. CS prepared the manuscript with contributions from all co-authors.

Declaration of Interest

The authors declare no competing financial and non-financial interest as outlined in the journal guideline.

Figures

Figure 1: A) Surface currents of the South Atlantic are indicated by white and blue arrows and labels, respectively (BC = Brazil Current; AC = Agulhas Current; SAC = South Atlantic Current; ACC = Antarctic Circumpolar Current; SAG = South Atlantic Gyre). Background color shows sea surface temperature recorded by the MODIS satellite at the time of cruise JC068. The Subtropical Front (STF) is indicated by the 16°C isotherm in grey. Trace metal stations are marked by black (JC068, St.1-3 and St.7-24) and grey circles (D357, St.1-6) and numbered from 1 to 24 (station numbers 10 and 23 were excluded). The location of the Rio de la Plata estuary on the South American shelf is indicated. B.) Salinity and C.) dissolved inorganic phosphorous (DIP) in µmol L^{-1} in the water column. The following water masses were identified: Sub-Tropical Surface Water (STSW), Sub-Antarctic Surface Water (SASW), Antarctic Intermediate Water (AAIW), Upper Circumpolar Deep Water (UCDW), North Atlantic Deep Water (NADW), Antarctic Bottom Water (AABW), and Weddell Sea Deep Water (WSDW). The location of the Argentine (west) and Cape (east) Basin are indicated.

Figure 2: A.) Dissolved lead (DPb) and B.) leachable particulate lead (LpPb) concentrations in pmol L^{-1} in the water column along the 40°S transect. Trace metal stations are marked from station 1 to 24 (Station numbers 10 and 23 were not used). LpPb values were available for cruise JC086 only. Water masses in Figure 2A correspond to water masses in Figure 1B & 1C.

Figure 3: Diagrams row A.) Left diagram: Concentration of dissolved (DPb) and leachable particulate lead (LpPb) in the water column on the shallow shelf (St. 24)). Right diagram: Salinity (black line) and transmittance in % (red line) of St. 24. Row B.) Similar to row A, but for deep

834 sea St. 20. C.) Relationship between DPb and LpPb in bottom waters on the shelf St. 24 (black
835 circles, regression 2), the deep sea for St. 20 (empty circle, regression 1) and St. 14 to St. 19, St.
836 21 and St. 22 (black triangles, regression 3). A linear regression and the R^2 for each set of data
837 has been included.
838
839 **Figure 4:** Box plot of the different water masses (similar to acronyms in Figure 1, but NADW in
840 the western (-w) and eastern basin (-e) are separated). The median of each water mass is
841 represented by the inner black line within each brown box. Upper and lower limit of the box
842 represent the 25% and 75% quartile. Whiskers indicate lowest and highest DPb concentration
843 applied for the box plot. Black crosses represent DPb values within the upper and lower whisker.
844 Black circles indicate outliers (not used for the box plot). Outliers above the box-whiskers-
845 statistics of AAIW, UCDW, NADW-w, AABW, and WSDW belong to results from St. 20. With
846 exception of St.24 the entire data set from cruise JC068 and D357 was used. The n-values for the
847 water masses are listed in Table 2.
848
849 **Figure 5:** (Upper panel) Shows model output for dissolved Pb (DPb) concentrations using the
850 eOMP analysis with DPb source water signatures for AAIW, NADW, and WSDW (Table 2).
851 (Lower panel) The residual in nmol L^{-1} represents the difference between modeled and measured
852 DPb concentration.

853 **Tables**

854 **Table 1:** Determined trace metal concentrations and standard deviation for n times analyzed
855 standard seawaters (SAFe S; SAFe D1 and D2; GS – GEOTRACES S; GD – GEOTRACES D).
856 The consensus value in grey for DPb is listed below the measured value. The analytical limit of
857 detection (LOD) and the method blank are at the right side of the table. More detailed
858 information about the used standard seawaters can be retrieved from the website:
859 *http://es.ucsc.edu/~kbruland/GeotracesSaFe/kwbGeotracesSaFe.html*

860

#	SAFe S	SAFe D1	SAFe D2	GS	GD	LOD	Blank
Pb (pmol L^{-1})	48.4 ± 6.1	23.9 ± 3.1	28.9 ± 4.4	26.9 ± 3.2	45.3 ± 0.3	0.6	2.8
Pb consensus	46.8 ± 2.1	27.0 ± 2.5	27.0 ± 1.5	27.8 ± 1.0	41.7 ± 1.5		
n =	25	5	19	6	3		

861

862 **Table 2:** Median water mass DPb concentrations for the 9 identified water masses (NADW-w
863 and –e are separated). Also included the 1st (25%) and 3rd (75%) quartile of the box plot statics
864 and the number of samples for each water mass.

865

#	Median DPb (pmol L-1)	Q1 (pmol L-1)	Q3 (pmol L-1)	n = samples
AC	22.7	21.8	23.4	22
BC	17.9	16.2	20.7	14
STSW	12.0	10.9	13.1	59
SASW	11.7	11.2	12.8	26
AAIW	10.8	10.2	11.5	43
UCDW	9.8	8.6	10.3	39
NADW –w (Argentine B.)	12.0	10.3	12.3	30
NADW-e (Cape B.)	8.1	7.4	9.0	21
AABW	6.0	5.0	6.8	22
WSDW	5.0	4.4	6.0	26

866

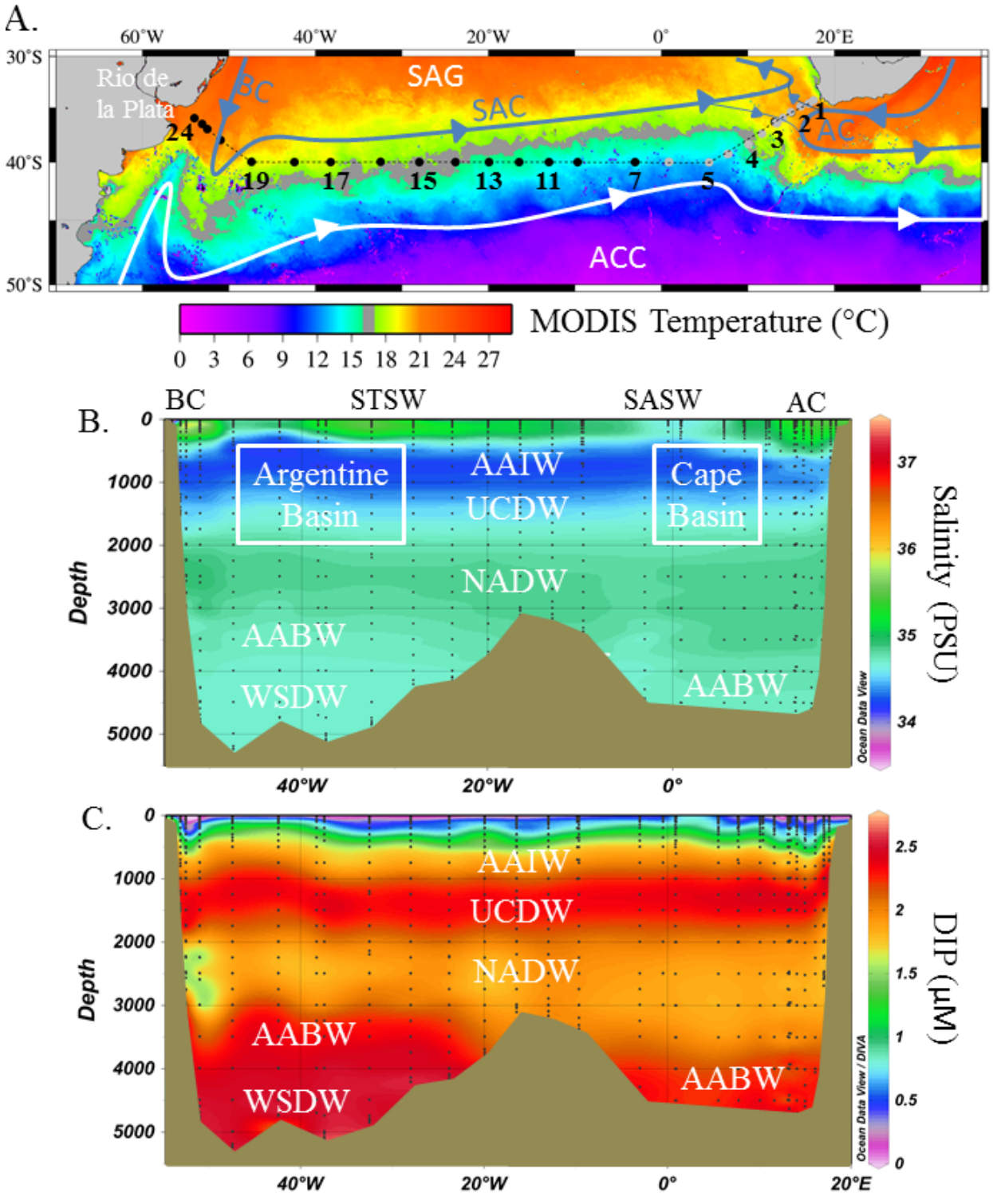
A.
60°W
40°W
20°W
0°
20°E
30°S
40°S
50°S
Rio de la Plata
BC
SAG
SAC
AC
ACC
24
19
17
15
13
11
7
5
4
3
2
1
MODIS Temperature (°C)
0 3 6 9 12 15 18 21 24 27
B.
BC
STSW
SASW
AC
Argentine Basin
Cape Basin
AAIW
UCDW
NADW
AABW
WSDW
AABW
Depth
0
1000
2000
3000
4000
5000
40°W
20°W
0°
Salinity (PSU)
37
36
35
34
Ocean Data View
C.
AAIW
UCDW
NADW
AABW
WSDW
AABW
Depth
40°W
20°W
0°
20°E
DIP (µM)
2.5
2
1.5
1
0.5
0
Ocean Data View / DIVA

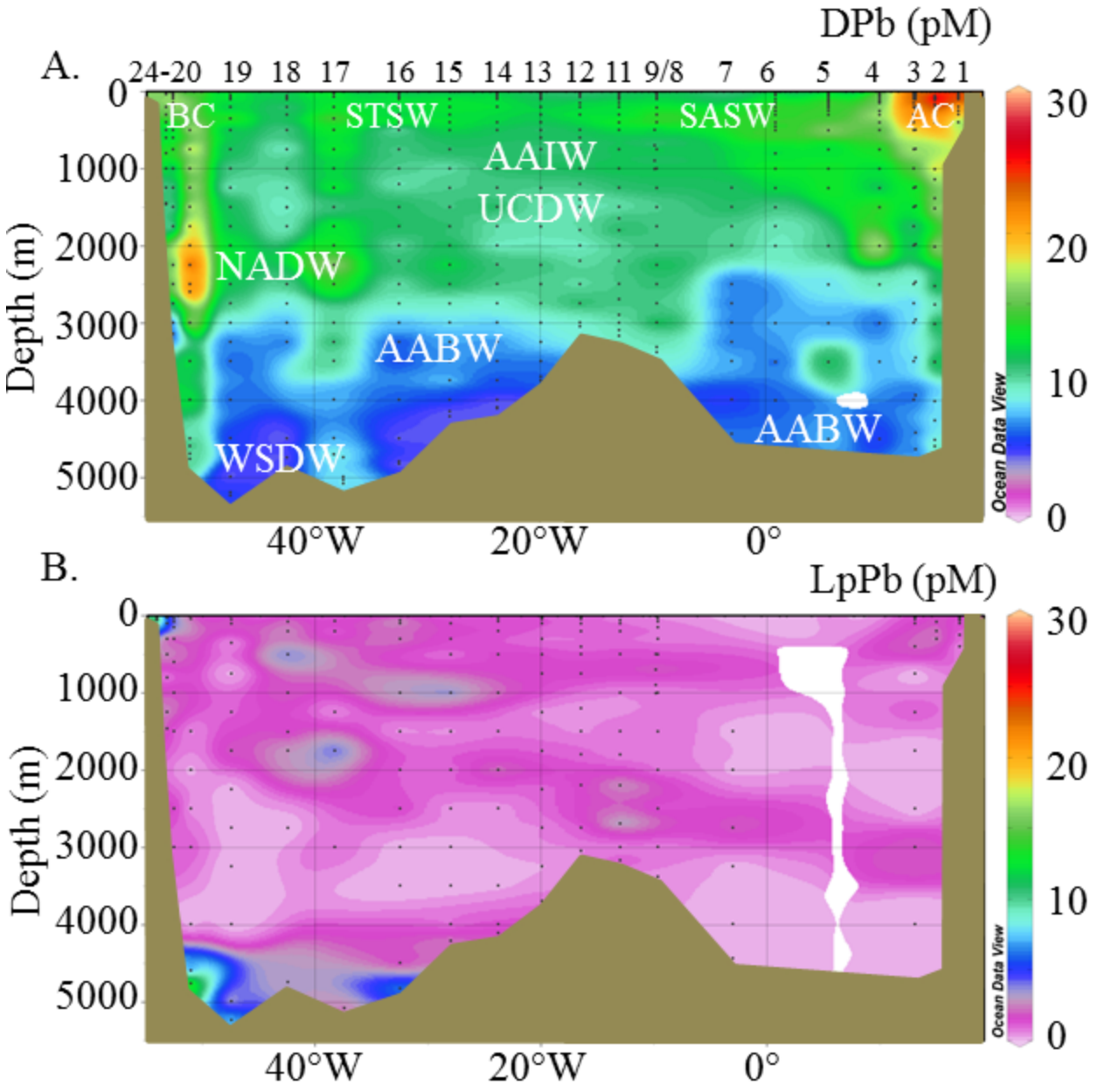
A.
DPb (pM)
24-20 19 18 17 16 15 14 13 12 11 9/8 7 6 5 4 3 2 1
BC
STSW
SASW
AC
AAIW
UCDW
NADW
AABW
AABW
WSDW
Depth (m)
0
1000
2000
3000
4000
5000
40°W
20°W
0°
30
20
10
0
Ocean Data View
B.
LpPb (pM)
Depth (m)
0
1000
2000
3000
4000
5000
40°W
20°W
0°
30
20
10
0
Ocean Data View

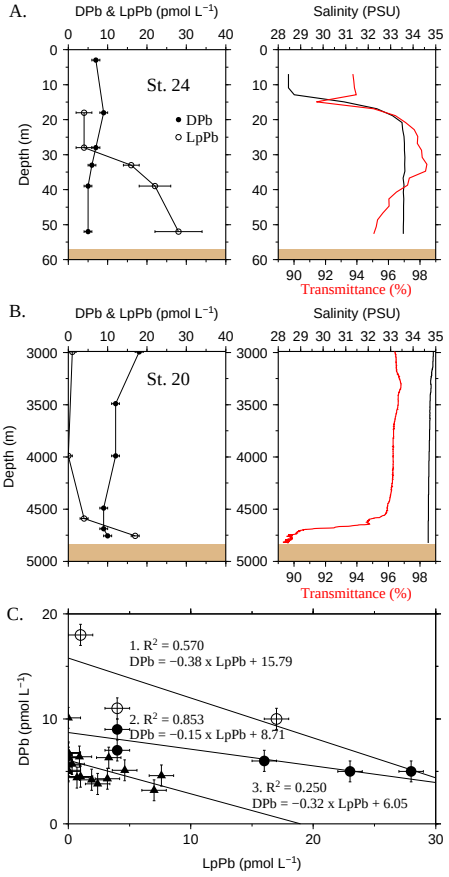

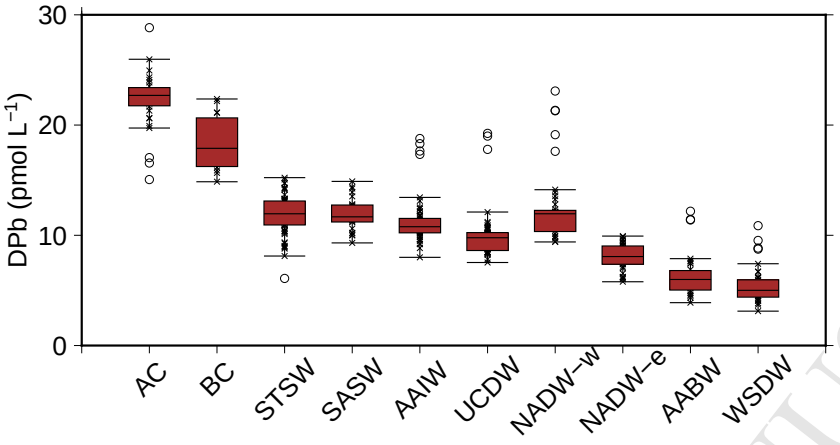

2

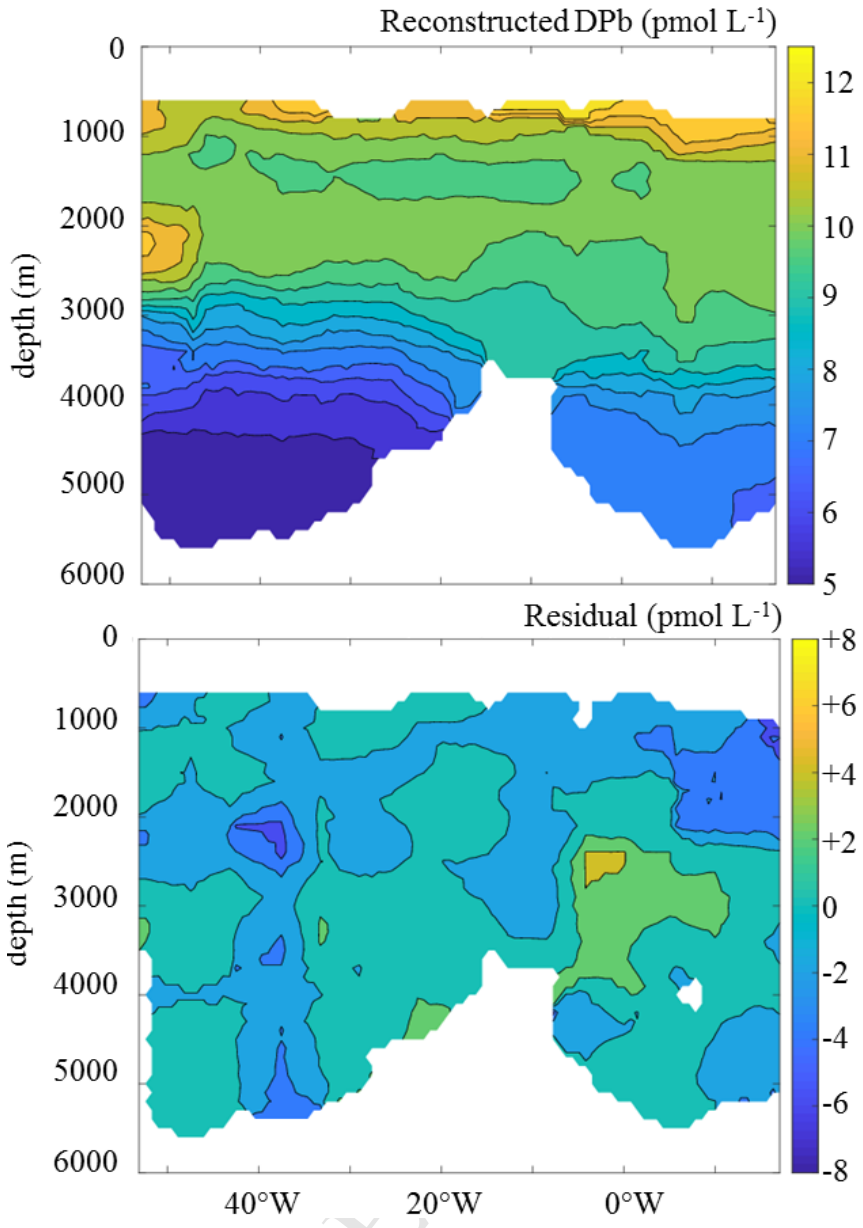

Research highlights

- Mineral sourced lead (Pb) accounts for circa 41% of the dissolved Pb pool
- Dissolved Pb in the surface ocean has a residence time of roughly 35 days
- Dissolved Pb is removed from seawater via particle scavenging processes
- Most water masses in the South Atlantic have distinct dissolved Pb concentration